Available online at www.sciencedirect.com
SCIENCE DIRECT®
ELSEVIER
Nuclear Instruments and Methods in Physics Research A 531 (2004) 18–37
NUCLEAR INSTRUMENTS & METHODS IN PHYSICS RESEARCH Section A
www.elsevier.com/locate/nima

Compound semiconductor radiation detectors

Alan Owens*, A. Peacock

Science Payload and Advanced Concepts Office (SCI-A), ESA/ESTEC, Postbus 299, 2200-AG Noordwijk, The Netherlands

Available online 11 June 2004

Abstract

We discuss the potential benefits of using compound semiconductors for the detection of X- and γ-ray radiation. While Si and Ge have become detection standards for energy dispersive spectroscopy in the laboratory, their use for an increasing range of applications is becoming marginalized by one or more of their physical limitations; namely the need for ancillary cooling systems or bulky cryogenics, their modest stopping powers and radiation intolerance. Compound semiconductors encompass such a wide range of physical properties that it is technically feasible to engineer a material to any application. Wide band-gap compounds offer the ability to operate in a wide range of thermal and radiation environments, whilst still maintaining sub-keV spectral resolution at hard X-ray wavelengths. Narrow band-gap materials, on the other hand, offer the potential of exceeding the spectral resolution of both Si and Ge, by as much as a factor of 3. Assuming that the total system noise can be reduced to a level commensurate with Fano noise, spectroscopic detectors could work in the XUV, effectively bridging the gap between the ultraviolet and soft X-ray wavebands. Thus, in principle, compound semiconductor detectors can provide continuous spectroscopic coverage from the far infrared through to γ-ray wavelengths. However, while they are routinely used at infrared and optical wavelengths, in other bands, their development has been plagued by material and fabrication problems. This is particularly true at hard X- and γ-ray wavelengths, where only a few compounds (e.g., GaAs, CdZnTe and HgI_2) have evolved sufficiently to produce working detection systems. In this paper, we examine the current status of research in compound semiconductors and by a careful examination of material properties and future requirements, recommend a number of compounds for further development. In the longer term, when material problems are sufficiently under control, we believe the future lies in the development of heterostructures and inserted interface layers to overcome contacting problems and quantum heterostructures and superlattices to facilitate low-noise readout.

PACS: 07.85.Nc; 81.05.Dz; 81.05.Ea; 81.05.Hd

Keywords: Compound semiconductors; X-rays; γ-Rays; Detectors

1. Introduction

The term compound semiconductor encompasses a wide range of materials, most of which crystallize in either the zincblende (ZB), wurtzite or rocksalt crystal structures. They were first investigated as radiation detectors in 1945 by

*Corresponding author. Tel.: +31-71-565-5326; fax: +31-71-565-4690.
E-mail address: aowens@rssd.esa.int (A. Owens).

0168-9002/$ - see front matter © 2004 Elsevier B.V. All rights reserved.
doi:10.1016/j.nima.2004.05.071

Van Heerden [1], who demonstrated that silver chloride crystals when cooled to low temperatures were capable of detecting γ-rays, α-particles and β-particles. This work was later extended to the thallious halides by Hofstadter [2] in 1949. Strangely, at this time, the elemental semiconductors were not anticipated to be responsive to radiation and it was not until several months later than McKay [3] managed to measure the polonium α-ray spectrum using a Ge surface barrier detector. While the subsequent development of Ge and Si radiation detectors was rapid, largely due to the explosive rise of the semiconductor industry, mixed-element and compound semiconductors, such as the alkali-metal halides, CdTe, CdZnTe and HgI_2, were plagued by material problems caused by severe micro-crystallinity, high defect densities, impurities and stoichiometric imbalances. Until the 1960s very little additional work was carried out and the reader is referred to the survey of Prince and Polishuk [4]. Since this time, progress has been incremental, but hardly spectacular and the reader is referred to the more recent review of McGregor and Harmon [5].

Compound semiconductors are generally derived from elements in groups II to VI of the periodic table. They are so useful because of the shear range of compounds available, compared to the elemental semiconductors, Sn-α, C, Si and Ge. Most elements in these groups are soluble within each other, forming homogeneous solid solutions. These solutions occur when atoms of a particular element are able to substitute a given constituent of a different material without altering its crystal structure. In order that atoms can form solid solutions over large ranges of miscibility, they should satisfy the Hume–Rothery rules, namely that,

- the two species have similar valencies,
- they have comparable atomic radii[1] allowing substitution without large mechanical distortion,
- their electronegativities are similar to avoid the creation of inter-metallic compounds, and
- individually, their crystal structures are the same.

[1] In fact, they should differ by no more than 15%.

In addition to binary materials (such as GaAs or InP), most compounds are also soluble within each other, making it possible to synthesize *ternary* (e.g., AlGaAs, HgCdTe) *quaternary* (e.g., InGaAsP, InGaAlP) and higher-order solutions, simply by alloying binary compounds together. This is illustrated graphically in Fig. 1 and the most common semiconductor materials tabulated according to group in Table 1. The main compound groups and how they are formed are described below. For completeness, we also include the elemental semiconductors.

- Group IV (B) elements: These are the classical elemental semiconductors, Si, Ge, C (diamond) and gray tin (α-Sn). Group IV elements are exceptional in the periodic table in that their outer shells are exactly half filled and thus can be filled by sharing electrons with four neighbors (i.e., a total of eight electrons). This allows lattice structures to be built up symmetrically without any preferred direction with a bonding that is purely covalent. One can also combine different group IV elements, e.g., SiC and SiGe, to produce compounds with intermediate properties. Other semiconductors are composed of two atoms, one from group $N(N<4)$ and the other from group $M(M>4)$, such that $N+M=8$.

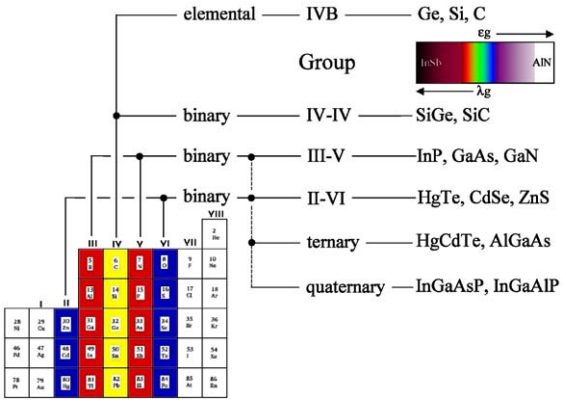

Fig. 1. Diagram illustrating the relationship of the elemental and compound semiconductors. Examples of compound type are given and are listed by increasing band-gap energy or alternately, decreasing wavelength, from the infrared to the UV. InSb and AlN delineate the extremes of the range in which compound semiconductors lie (0.17 eV to 6.2 eV).

Table 1
Common semiconductor materials

Band-gap energy (eV)	Elemental group IVB	Binary IV–IV compounds	Binary III–V compounds	Binary II–VI compounds	Binary IV–VI compounds	Binary *n*-VIIB compounds	Ternary compounds
0.00–0.25	Sn		InSb	HgTe			HgCdTe
0.25–0.50			InAs	HgSe	PbSe, PbS, PbTe		
0.50–0.75	Ge		GaSb				InGaAs
0.75–1.00		SiGe					
1.10–1.25	Si						
1.25–1.50			GaAs, InP	CdTe			AlInAs
1.50–1.75			AlSb	CdSe			AlGaAs
1.75–2.00			BP, InN				CdZnTe, CdZnSe, InAlP
2.10–2.25		SiC	AlAs	HgS		HgI_2	CdMnTe
2.25–2.50			GaP, AlP	ZnTe, CdS		PbI_2	TlBrI, InAlP, $TlPbI_3$
2.50–2.75				ZnSe		TlBr	
2.75–3.00				MnSe			
3.10–3.25				MnTe			
3.25–3.50			GaN	MgTe, MnS			
3.50–3.75				MgSe, ZnS			
3.75–4.00							
4.10–4.25							
4.25–4.50				MgS			
4.50–4.75							
4.75–5.00							
5.10–5.25							
5.25–5.50	C						
5.50–5.75							
5.75–6.00			BN				
6.10–6.25			AlN				
6.25–6.50							
6.50–6.75							
6.75–7.00							

Note: Compounds are listed in order of increasing band-gap energy.

- Group III–V compounds: Compound semiconductors combining an anion from group V (from nitrogen on down) and a cation from group III (usually, Al, Ga or In). Each group III atom is bound to four group V atoms and vise versa—thus each atom has a filled (eight electron) valence band. Although the bonding would appear to be entirely covalent, the shift of valence charge from group V atoms to group III atoms induces a component of ionic bonding to the crystal. When grown epitaxially (molecular beam epitaxy (MBE), metal organic chemical vapor deposition (MOCVD) and variants), they usually assume a ZB structure. The stable bulk allotrope often has a wurtzite structure.

Ternary III–V alloys have the general form $(A1_x, A2_{1-x})B$ with two group III atoms used to fill group III atoms in the lattice) or $A(B1_x, B2_{1-x})$ using two group V atoms in group V atomic positions in the lattice. Here A and B represent elements from group III and V, respectively. The quaternary semiconductors use two group III and two group V elements yielding a general form $(A1_xA2_{1-x})(B1_y, B2_{1-y})$ for $0<x<1$; $0<y<1$—for example, $Ga_{0.12}In_{0.88}As_{0.23}P_{0.77}$.

- Group I–II–V compounds: Semiconductors that are sometimes thought of as derivative of the III–V's, with a monovalent–divalent species pair replacing group III metal. An example would be LiZnAs.
- Group I–III–VI compounds: Chalcopyrites like $CuInSe_2$. Instead of bonding to four group II elements as in a II–VI semiconductor, the group VI element bonds to two group I and two group III elements in the I–III–VI_2 ternary system. Cu–In–Se systems are the most studied variants at this time, especially the alloy $CuIn_{1-x}Ga_xSe_2$ $(Cu(In, Ga)Se_2)$. I–III–VI systems offer direct-gap semiconductors over a broad range of lattice constants and band gaps and are presently being investigated for exploitation as photovoltaic materials.
- Group II–VI compounds: A compound of a IIb metal (e.g., Zn, Cd and Hg, in periods 3, 4 and 5, respectively) with a group VIa cation. The latter is usually S, Se or Te. Compounds generally crystallize naturally in a hexagonal or NaCl structure. Pseudo-binary alloys with Mn, Zn and Se are also common, e.g., $Cd_{(1-x)}Mn_xTe$, $Cd_{(1-x)}Zn_xTe$ and $Cd_{(1-x)}Se_xTe$. II–VI compounds typically exhibit a larger degree of ionic bonding than III–V materials, since their constituent elements differ more in electron affinity due to their location in the periodic table. A major motivation to study II–VI semiconductors is their broad range of band gaps (from 0.15 eV for HgTe to 4.4 eV for MgS), high effective Z and the demonstrated possibility of making MBE and MOCVD grown heterostructures, as for III–V systems. II–VI semiconductors can also be created in ternary and quaternary forms, although less common that III–V varieties.
- Group I–VII compounds can also form semiconductors, which exhibit a very large ionicity and energy gaps considerably larger than many III–V compounds: The latter is a direct consequence of the fact that bonding in these materials is almost entirely ionic and not covalent as in VI–VI, III–IV and most II–VI materials. Specific examples include the silver halides, AgCl and AgBr, which were some of the first compound semiconductors demonstrated to be sensitive to ionizing radiation.
- Group I–IV, I–V–VI and other organic (polymer, oligomers) derivatives: These are the so-called "plastic" semiconductors. They are polymers with a de-localized π-electron system along the polymer backbone. This results in the creation of alternating single and double bonds by weak pz–pz bonding, which in turn results in the creation of a band gap ($\sim$2.5 eV). At present, organic materials are being exploited for use in low-cost flexible displays and low-end data storage media. Such materials offer numerous advantages in terms of easy processing (spin coating as opposed to epitaxial growth), and good compatibility with a wide variety of substrates.

From the above categories we can make several generalizations. For example, we note a clear tendency for the band-gap energy and melting point to increase with increasing ionicity (i.e., going from group IV to III–V through to II–VI and finally to group I–VII compounds), while micro-hardness decreases. There is also a clear tendency for the band-gap energy to decrease with increasing lattice constant by roughly a factor of 2 Å. This is true for all groups, except group I–VII materials, which show little variation.

As with all semiconductors, the basic problem in producing compounds is the difficulty of growing chemically pure and structurally perfect crystals with exact stoichiometry. The most significant constraint in forming higher-order alloys is the lattice-mismatch or strain between layers. Changing the composition of an alloy changes its average lattice constant to reflect the different atomic bonding radii of the constituent elements. Stable alloys can only be formed if the change in

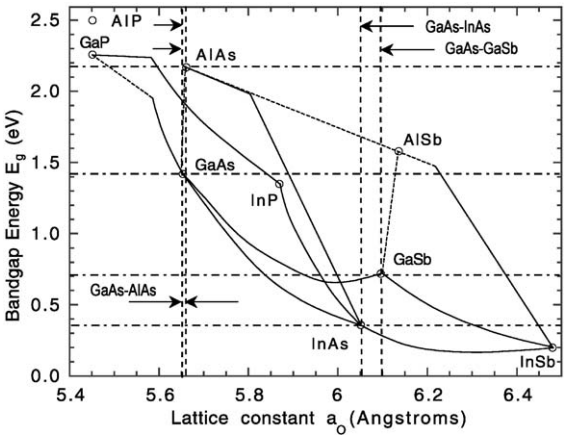

Fig. 2. Band-gap energy, E_g, versus lattice constant, a_0, for the most common III–V binary compounds at room temperature and their relationship to higher order alloys. The solid interconnect lines represent direct band-gap compounds while the dotted interconnect lines represent indirect band-gap compounds.

lattice constant is kept to less than 15%. In Fig. 2, we plot band-gap energy versus the cubic lattice constant for the most common III–V binary compounds. For a possible range of ternary alloy systems, a solid line is generated between the participating binaries (in the case of a quaternary compound, the boundary is laid out by four intersecting lines). Thus, we see for the GaAs–AlAs system, there is little variation in lattice constant,[2] which allows the formation of solid solutions of Al in GaAs over the full range of Al substitution. However, for the GaAs–InAs and GaAs–GaSb systems, the incorporation of In to GaAs (to form the $Ga_{(1-x)}In_{(x)}As$ alloy) or Sb to GaAs (to form the $GaAs_{(1-y)}Sb_{(y)}$ ternary alloy) results in major shifts of the average lattice constant and stable alloys cannot be produced across the entire range of In or Sb substitution. Fortunately, lattice-mismatched layers can be grown pseudo-morphically (that is, defect-free) on a substrate with a different lattice constant if the layer thickness is kept below a certain critical value. With the advent of modern epitaxial growth techniques, such as MBE and MOCVD, the composition of semiconductor layers can now be controlled to a scale of one monolayer (that is, an atomic bi-layer for compound semiconductors), or roughly $\sim 3\,\text{Å}$. Thus, it is literally possible to build up a semiconductor device one atomic layer at a time.

The Science Payload and Advanced Concepts Office of ESA has an extensive laboratory program to develop custom X- and γ-ray detection systems for future ESA space missions. These systems have to operate in a variety of diverse and esoteric environments; ranging from the relatively benign and stable near-Earth orbit environment to the hostile radiation environments of the Jovian system—the corrosive atmosphere of Venus—or the extreme thermal environment of Mercury. Because of this, our research has largely concentrated on compound semiconductors for reasons that will be elucidated below.

2. Radiation detection using compound semiconductors

All semiconductor detectors operate as solid-state ionization chambers and as such detect the charged particles produced by photon interactions. The choice of which compound to use for a specific application depends to a large extent on the energy range of interest. X- and γ-rays interact with matter primarily through three mechanisms. These are: (1) the photoelectric effect, in which the photon transfers all its energy to an atomic electron; (2) the Compton effect in which the photon interacts with an outer electron but only transfers a fraction of its energy to it, producing a hot electron and a degraded photon; and (3) pair production in which a photon above a threshold energy of $2m_0c^2$ interacts within the Coulomb field of the nucleus producing an electron and positron pair. Only the photoelectric effect leads to the total absorption of the incident energy, since a Compton scattered photon or an electron–positron pair (or its interaction products) may escape the detection volume and subsequently not deposit all of their energy within the detector. In general, the photoelectric effect dominates in the energy region up to $\sim 200\,\text{keV}$, the Compton effect up to a few MeV and pair production above $\sim 6\,\text{MeV}$. For a given compound, let N be the number of atoms per unit

[2] The actual mismatch between GaAs and AlAs is 0.127%.

volume and Z its effective atomic number. The interaction cross-sections vary as NZ^5 for the photoelectric, NZ for Compton scattering and NZ^2 for pair production. Thus, it can be seen that for good spectroscopy at γ-ray energies, one should choose the highest possible Z, since this increases the energy range over which total energy absorption can occur due to the photoelectric effect. However, for compounds, absorption is generally most influenced by the element with the highest atomic number, rather than the compounds average Z. For example, while both GaAs and InP have the same average Z of 32, the absorption coefficients of InP are two to three times higher in the hard X-ray region, purely due to the higher Z of In, i.e., 49 as opposed to 31 for Ga and 33 for As. This factor falls approximately as a power law of energy index ~ -0.3. However, even at 1 MeV the attenuation coefficients of InP are still 3% higher than GaAs.

Ionizing radiation absorbed in the material excites electron–hole pairs in direct proportion to the energy deposited (i.e., $n = E_0/\varepsilon$, where n is the number of electron–hole pairs generated, E_0 is the energy deposited and ε is the *average* energy consumed to create an electron–hole pair). Once charge has been generated the next problem is collection. Applying an electric field across the detector causes the liberated carriers to drift toward the anode and cathode with drift velocities v_e and v_h, creating an induced charge on the electrodes as described by the Shockley–Ramo theorem [6,7]. Integration of this charge gives the total charge, Q. In the case when trapping can be ignored, $Q = Q_0$, the initially created charge, which in turn is proportional to the energy of the incident photon. However, in any semiconductor some density of electron and hole traps are always present and these result in a loss of carriers and therefore a charge at the electrodes. In the case of a uniform electric field and negligible de-trapping, the fraction of charge that reaches the electrodes, or alternately, the charge collection efficiency (CCE), is given by the Hecht equation [8]:

$$\mathrm{CCE} = \frac{Q}{Q_0} = \frac{\lambda_e}{L}\left[1 - \exp\left(-\frac{(L - x_0)}{\lambda_e}\right)\right] + \frac{\lambda_h}{L}\left[1 - \exp\left(-\frac{x_0}{\lambda_h}\right)\right] \quad (1)$$

where L is the detector thickness, x_0 is the distance from the cathode to the point of charge creation and λ_e and λ_h are the carrier drift lengths in the applied electric field given by, $\lambda_e = \tau_e \mu_e E$ and $\lambda_h = \tau_h \mu_h E$. Here, τ_e and τ_h are the electron and hole lifetimes and μ_e and μ_h are the corresponding mobilities to which the drift velocities are related via $v_e = \mu_e E$ and $v_h = \mu_h E$. Thus, it follows from Eq. (1) that the CCE depends not only on λ_e and λ_h, but also on the location where the charge was created. Since the interaction points of incident photons are essentially random, being weighted by the classical exponential absorption law, the width of the peak in the energy spectrum broadens to a degree governed by the ratios λ_e/L and λ_h/L. Strictly, this width can only be realistically evaluated by following the approach of Trammell and Walter [9] in which the individual pulse heights in infinitesimal slices through the detector are summed over the detector thickness. However, in addition to broadening caused by poor charge collection, the width of the full energy peak, ΔE, is also broadened by the statistics of carrier generation (or Fano noise) and by electronic noise. Fano noise is influenced mainly by the electron–hole pair energy, whereas electronic noise is dominated by the detector leakage or dark current and the noise generated in the front-end components of the preamplifier (e.g., input FET). Thus, the resulting energy resolution, ΔE, of a detection system at energy E_0 will be given by the convolution of the probability distributions of these components.

$$\Delta E = f(\sigma_F^2,\ \sigma_e^2,\ \sigma_c^2) \quad (2)$$

where σ_F^2 is the variance of the noise due to carrier generation, or Fano noise, σ_e^2 is the variance of the noise due to the leakage current and amplifier noise and σ_c^2 is the variance of the noise due to incomplete charge collection due to carrier trapping. For most compound semiconductor detectors, ΔE can be reasonably well described by the semi-empirical function,

$$\Delta E = 2.355\sqrt{F\varepsilon E_0 + (\Delta e/2.355) + a_1 E_0^{a2}} \quad (3)$$

where F is the Fano factor, Δe is the measured FWHM of the electronic noise and a_1 and a_2 are semi-empirical constants determined by best-fitting.

In general, Fano and electronic noise are less important than the noise due to incomplete charge collection, except for thin detectors where $\lambda_e/L \gg 1$.

2.1. Compound semiconductors and radiation detection

For radiation detection, compound semiconductors have a number of distinct advantages over their elemental counterparts, arising from the wide range of stopping power and band gaps available. For example, within a given target spectral resolution and detection efficiency, it is usually possible to select from a range of stopping powers. Choosing materials with the largest stopping powers enables thinner detectors to be produced with resulting benefits in radiation tolerance (which is a bulk effect) and lower leakage currents. Alternatively, choosing smaller stopping powers will increase scattering efficiency, which is a requirement for polarimetry, or say, the upper detection plane of a double Compton telescope. By careful choice of both band gap and stopping power it is possible to fabricate detectors with a very wide dynamic range but sub-keV energy resolution in the soft X-ray band and tens of keV in the γ-ray band. For space research this is particularly attractive, since it has mass and cost benefits in spacecraft design in that by using denser materials smaller detection systems can be fabricated without losing spectral acuity. Finally, unlike Si and Ge whose electronic and chemical properties are "fixed", those of compound semiconductors can be modified by band-gap engineering [10].[3] Specifically, the energy gap between the valence and conduction states is defined by the inter-atomic distance and the electronegativity of the component atoms. Changing the composition of an alloy, changes its average lattice constant to reflect the different atomic bonding radii of the chemical elements making up the crystal. This changes the band-gap energy, which in turn alters the properties of the material. A specific example of how this is useful for radiation detector applications is CdZnTe. In Fig. 3, we plot the band-gap energy as a function of lattice constant for a range of II–VI materials, including CdTe and ZnTe. By altering the zinc fraction, x, in $Cd_{(1-x)}Z_xTe$, the range of possible alloys moves along the line between CdTe and ZnTe, making it is possible to optimize the noise performance of a CdZnTe radiation detector for a given operating temperature. Specifically, increasing the zinc fraction, x, increases the band-gap energy E_g, which can be described empirically [11] by

$$E_g(x) = 1.510 + 0.606x + 0.139x^2 \text{ eV}. \quad (4)$$

While an increase in E_g increases Fano noise due to carrier generation statistics, it simultaneously reduces shot noise due thermal leakage currents. A trade-off can lead to a noise minimum at a given operating temperature and therefore an optimization of the spectral performance [12]. For example, a zinc fraction of 10% is optimum for operation at -30°C, whereas 70% is optimum at room temperature. Alloying of CdTe with Zn or ZnTe has additional benefits in that it increases the energy of defect formation [13] and mechanically strengthens the lattice with a resulting lowering of defect densities [14].

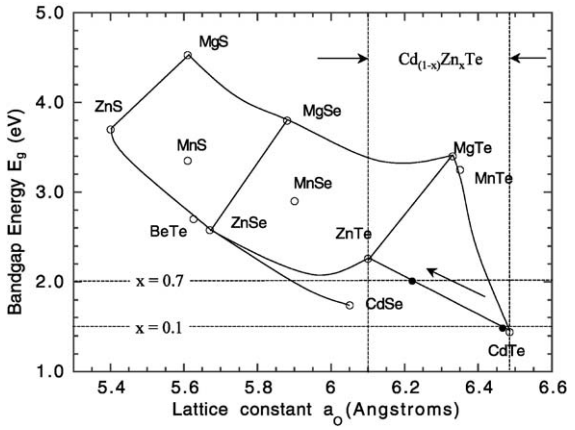

Fig. 3. Band-gap energy, E_g, of II–VI compounds as a function of lattice constant a_0. The dotted lines illustrate how altering the zinc fraction, x, in $Cd_{(1-x)}Zn_xTe$ alters the band-gap energy. Two cases are shown: $x = 0.1$ which provides optimum energy resolution at $T = 243$ K, and $x = 0.7$ which provides optimum energy resolution at room temperature (see text).

[3] Or, alternatively, wavelength engineering. In this case, the ability to tailor the band gap to a particular wavelength has profound opto-electronic applications.

2.2. Targeting compounds for specific problems

In principal compound semiconductors can also be matched to (a) specific applications or (b) specific environments. As an example of (a), we note that GaAs would be an ideal material for use in planetary X-ray fluorescent spectrometers or solar X-ray monitors, since, unlike silicon, gallium and arsenic do not occur naturally in the source spectra and both the Ga and As absorptions edges lie well outside the energy range of interest. This makes the interpretation of spectra considerably easier. Other suitable materials include CdTe and PbI_2. With regard to (b), materials can be selected to operate at elevated temperatures, in harsh radiation environments or even in corrosive atmospheres (e.g., applications in nuclear redemption, chemical processing, well logging). Specific materials that could be used in these areas are HgI_2, SiC and CVD diamond. Whilst diamond is not a compound semiconductor, we treat it as such, because it has great potential in many specialized areas and its development has been plagued by exactly the same problems.

In Table 2, we list the physical, electrical and transport characteristics of a number of compound semiconductors for which spectroscopic results at X- and γ-ray wavelengths have been reported. In Fig. 4, we show the intrinsic energy resolution that is potentially achievable as a function of band-gap energy for a range of compound semiconductors assuming an average value for the Fano factor of 0.14. For completeness we also include the superconductors. The temperature ranges in which different compounds can be expected to operate are illustrated on the left-hand side of the figure, from which we can see that room temperature operation can only be achieved for band gaps above ~ 1.4 eV, while thermoelectric cooling can be used for Si down to Ge. At and below Ge, cryogenic cooling is required. We thus define wide band-gap (WBG) semiconductors as having a band-gap energy conducive to room temperature operation, i.e., > 1.4 eV and narrow band-gap (NBG) compounds having a band-gap energy below this value. Whilst narrow-gap compounds offer the potential of energy resolutions surpassing Si or Ge, at the present time, spectroscopic detectors have only been produced for compounds with band-gap energies greater than 1.35 eV. Recently, however, there has been the first report of the detection of 5.8 MeV α-particles by the NBG material, InSb, operated at a temperature of below 4.2 K [15].

3. Limitations of compound semiconductors

Unfortunately, compound semiconductors also suffer from several limitations, which do not affect their elemental counterparts. Perhaps the most severe of which is that one or both charge carriers suffer from poor transport—either through poor mobility or carrier lifetime. In this regard, the most useful figure of merit when comparing compounds is the mobility–lifetime product ($\mu\tau$). For the elemental semiconductors this is of the order of unity for both electrons and holes, whereas for compound semiconductors it rarely reaches greater than a few times 10^{-4} for electrons and 10^{-5} for holes—and these figures get worse with increasing Z. The cause can usually be traced to trapping centers caused by impurities, lack of stoichiometry, or for the softer materials, plastic deformation caused by mechanical damage during fabrication. Poorer $\mu\tau$ products result in short drift lengths, which in turn, limit the maximum size and therefore energy range of detectors. Some improvement can be made by utilizing single carrier collection techniques such as pulse rise time discrimination [16], Frisch grids [17], or in the case of pixel detectors, by careful design (i.e., exploiting the small-pixel effect [18]).

Transport problems are exacerbated by the fact that there are no native III–V oxides and a very limited choice of doping agents. This makes surface passivation difficult and precludes the creation of metal–dielectric–semiconductor structures on NBG materials. The fabrication of stable and laterally uniform contacts is also a problem, since the choice of suitable materials is severely limited for most compounds. Additionally, the quality of the contacts, can significantly affect a detectors performance. Metal–semiconductor contacts can be either ohmic or Schottky. Simply stated, Schottky contacts imply a Schottky barrier

Table 2
Compilation of the physical properties of compound semiconductors for which spectroscopic results have been reported, grouped according to density

Parameter	Si	4H-SiC	InP	GaAs	Ge	$Cd_{0.35}Mn_{0.55}TeCd_{0.7}Zn_{0.3}SeCd_{0.9}Zn_{0.1}TeCdSe$				CdTe	PbI_2	HgI_2	TlBr
Density ($g\,cm^{-3}$)	2.33	3.21	4.78	5.32	5.33	5.8	5.5	5.78	5.81	5.85	6.2	6.4	7.56
Average atomic number(s)	14	10	32	31.5	32	49	38	49.1	41	50	63	62	58
Band gap (eV)	1.12	3.26	1.35	1.43	0.67	1.73	2.0	1.572	1.73	1.44	2.32	2.15	2.68
Pair creation energy (eV)	3.62	7.8	4.2	4.2	2.96	2.12	6.0	4.64	5.5	4.43	4.9	4.2	6.5
Electron mobility ($cm^2\,V^{-1}\,s$)	1400	1000	4600	8000	3900			1000	840	1100	8	100	30
Hole mobility ($cm^2\,V^{-1}\,s$)	1900	115	150	400	1900		10	120	75	100	2	4	4
Electron lifetime (s)	$>10^{-3}$	5×10^{-7}	1.5×10^{-9}	10^{-8}	$>10^{-3}$			3×10^{-6}	10^{-7}	3×10^{-6}	10^{-6}	3×10^{-6}	2.5×10^{-6}
Hole lifetime (s)	10^{-3}	7×10^{-7}	$<10^{-7}$	10^{-7}	2×10^{-3}	10^{-7}	10^{-7}	1×10^{-6}	10^{-6}	2×10^{-6}	3×10^{-7}	1×10^{-5}	3.7×10^{-5}
Electron $\mu\tau$ product ($cm^2\,V^{-1}$)	>1	4×10^{-4}	5×10^{-6}	8×10^{-5}	>1	$>10^{-6}$	$\sim10^{-4}$	4×10^{-3}	6.3×10^{-5}	3×10^{-3}	1×10^{-5}	3×10^{-4}	5×10^{-4}
Hole $\mu\tau$ product ($cm^2\,V^{-1}$)	~1	8×10^{-5}	$<1.5\times10^{-5}$	4×10^{-6}	>1		10^{-6}	1.2×10^{-4}	7.5×10^{-5}	2×10^{-4}	3×10^{-7}	4×10^{-5}	2×10^{-6}
Crystal structure	Cubic	Hexagonal	Cubic (ZB)	Cubic (ZB)	Cubic	Hexagonal	Hexagonal	Cubic (ZB)	Wurtzite	Cubic (ZB)	Hexagonal	Tetragonal	Cubic (CsCl)
Lattice constant (Å)	5.43095	3.079 (a) 5.048 (c)	5.8686	5.6533	5.64613				4.2999 (a) 7.0109 (c)	6.48		4.37 (a) 12.44 (c)	3.47
Knoop hardness ($kg\,mm^{-2}$)	1150	2540	460	750	692			?	90–130	60	<10	<10	12
Melting point (°C)	1412	2827	1060	1238	958	1080	1320	1092–1295	1239	1092	408	259	460
Dielectric constant	11.7	9.7	12.4	12.8	16			10	10.2	10.9		8.8	29.8
Resistivity (Ω/cm)	$<10^4$	$>10^5$	10^6	10^7	50	10^{10}	10^{10}	3×10^{10}	10^9	10^9	10^{13}	10^{13}	10^{12}
$1/e$ abs. Depth (mm) at 10 keV	0.127	0.128	0.020	0.051	0.050	0.019	0.019	0.011	0.019	0.011	0.011	0.011	0.011
at 100 keV	23.30	17.90	1.597	3.46	3.51	1.5	1.5	1.01	1.5	1.01	0.453	0.46	0.32
Typ. FWHM ΔE (keV) at 60 keV	0.4	2.7	12	0.7	0.3	21	1.8	1.5	8.5	1.1	1.83	3.5	7.9
Intrinsic. FWHM ΔE (keV) at 60 keV (Fano noise)	0.415	0.642	0.443	0.439	0.250	0.530	0.530	0.393	0.506	0.300	0.441	0.409	0.550
Typical thickness (mm)	0.3	0.3	0.2	0.2	20	0.5	0.1	2	0.5	2	0.1	10	1

Note: For comparison, the properties of the elemental semiconductors, Si and Ge are also listed. The Fano noise was calculated using the "best" reported values of the Fano factor, otherwise a value of 0.14 was assumed.

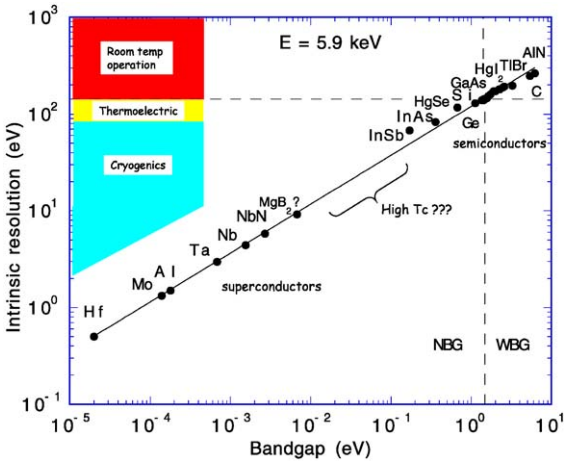

Fig. 4. The limiting energy resolution achievable for a range of compound semiconductors as a function of band-gap energy at 5.9 keV. For completeness we also include the superconductors. Curves are given for average values of the Fano factor, i.e., 0.22 for superconductors and 0.14 for semiconductors. NBG and WBG show the regions in which the narrow band gap and wide band gap semiconductors lie.

and the current–voltage characteristics display rectifying behavior, whereas ohmic contacts imply no barrier and the current voltage characteristics are linear (i.e., there is an unimpeded transfer of majority carriers from one material to another). For a general review, see Ref. [19].

It is difficult to form ohmic contacts to WBG materials[4] because there are few metals that satisfy the work function requirements necessary to remove the energy barrier to carrier flow. Specifically, at the interface between the contact and the semiconductor, their respective Fermi-levels will equalize and current will flow across the barrier providing the work function of the metal contact is less than that of the semiconductor (i.e., $\phi_m < \phi_s$) for n-type material (the converse is true for p-type material). Unfortunately it is difficult, if not impossible to find metals with a suitably small ϕ_m when using WBG n-type (or large ϕ_m for p-type) semiconductors. For these materials, a contact scheme is selected which relies on quantum mechanical tunneling of the carriers through the energy barrier, in other words by controlling the barrier width rather than its height. This can be achieved if (a) the potential barrier is sufficiently small and (b) high levels of doping ($>10^{17}$) are employed. On top of all the previous considerations, special metallization schemes may also be required if the device is to operate in unusual or harsh environments. Lastly, the above situation is further complicated by stoichiometric and impurity issues, in that, the surface energy states introduced by precipitations, dislocations and interfaces, can effectively pin the Fermi-level making the barrier height essentially independent of the contact work function. It is found experimentally that Schottky barrier heights (SBHs) for a wide range of metals on a particular semiconductor fall within a narrow range. In fact, this range is so narrow that it is described empirical by the "one-third" rule, i.e., the SBH is roughly $\frac{1}{3}$ of the band gap in a p-type semiconductor and $\sim\frac{2}{3}$ of the band gap in an n-type semiconductor. Thus, the Fermi-level appears to be fixed, or "pinned" at $E_g/3$ from the valence band maximum. The effect is found to be dependent to a large extent on the type of bonding. For example, surface pinning tends to be more prevalent in covalently bonded compounds than ionically bonded compounds and therefore is also related to the electronegativity of a compound, since covalent substances tend to be less electronegative than ionic. Thus, with reference to Section 1, we would expect pinned surfaces to be more common in III–V materials rather than II–VI or I–VII compounds. Most recently, it has been shown that Fermi-level pinning is actually a natural consequence of interfacial bonding, in that the penetration of metal induced gap states is deeper in covalent semiconductors than in ionic semiconductors and, hence, these states more effectively screen-out changes in the metal work function in a covalently bonded material. General procedures for forming ohmic contacts to "pinned" compounds may be found in Kim and Holloway [20]. For III–V compounds, the survey of Baca et al. [21] discusses contacting materials and properties as well as critical material issues pertaining to representative III–V compounds.

[4] For a general discussion and review of ohmic contacts to II–VI and III–V materials the reader is referred to Kim and Holloway [20].

4. Present detection systems

Two and a half decades ago, Armantrout et al. [22] produced a rank-ordered listing of the most promising materials for further development. However, out of a list of nine compounds, only CdSe, HgI_2 and CdTe were investigated and of these only HgI_2 and CdTe are still under active development. Even so, CdTe is used in less and less applications as CdZnTe has largely superseded it in view of its higher resistivity, lower dislocation density and lower susceptibility to polarization effects. At the present time only GaAs, CdZnTe and HgI_2 have evolved sufficiently enough to produce efficient soft and hard X-ray detection systems and as such, we will not discuss them further other than to show the spectral responses of comparatively sized monolithic detection systems to ^{241}Am and ^{55}Fe radioactive sources (see Fig. 5). For comparison we also show the response of a reference Si detector. Rather, we will concentrate on the development of several promising, but as yet immature compounds.

Silicon carbide (SiC) is currently being explored as a high-temperature Si alternative that is also chemical and radiation tolerant. It has several distinct advantages over Si, in that it has twice the thermal conductivity and eight times the maximum breakdown field. The former property is important for producing thermally stable or high-power semiconductor devices, while the latter means that much higher biases can be applied, resulting in higher drift velocities and better charge collection. SiC belongs to a family of materials which display a one-dimensional (1-D) polymorphism called polytypism. Polytypes differ by the stacking sequence of each tetrahedrally bonded Si–C bilayer, crystallizing into either cubic, hexagonal or rhombohedral structures. Although over 200 polytypes have been discovered, three are generally considered—4H-SiC (hexagonal), 6H-SiC (hexagonal) and 3C-SiC (face centered cubic), of which the first has the best electronic properties. At present, the X-ray performance of prototype detectors are still relatively poor, with FWHM resolutions of 2.7 keV at 59.54 keV being reported [24]. However, recent measurements using very small-pixel detectors have achieved room temperature energy resolutions of 693 eV at 59.54 keV [25].

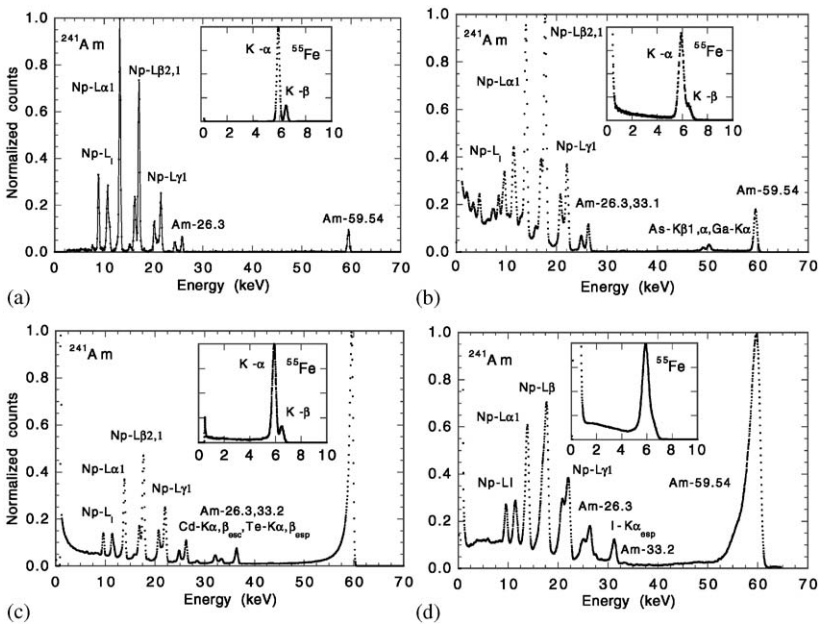

Fig. 5. Measured ^{241}Am and ^{55}Fe energy-loss spectra in (a) 1 mm^2, 500 μm thick Si detector, (b) 1 mm^2, 40 μm thick GaAs detector, (c) 3.142 mm^2, 2.5 mm thick CdZnTe detector and (d) 7 mm^2, 500 μm thick HgI_2 detector [23].

Similarly, CVD diamond has been proposed for use in hostile, hot, corrosive and/or very high radiation environments [26]. In medicine, CVD diamond is ideal for use in hadron therapy dosimetry in view of the high radiation gradients encountered and particularly its tissue equivalence, alleviating the need for dose corrections. Diamond is a carbon allotrope, bonded tetrahedrally in the diamond cubic lattice structure (two interpenetrating face centered cubic lattices with a displacement of one quarter body diagonal). This bond structure in conjunction with carbons low atomic number, gives diamond the highest atom density of any material, which in turn is responsible for many of its superlative properties. It is chemically inert, strong, extremely hard and an excellent thermal conductor. Initial studies show that both natural and CVD material respond to radiation and are extremely radiation hard [27], but are not spectroscopic at this time [28].

InP has been investigated because its structural and electronic properties are similar to Si and GaAs, but with one of the highest electron mobilities of any semiconductor material (in fact ~ 3 times that of silicon). This makes it a particularly attractive material for high-count rate applications. InP can be alloyed to GaAs and therefore it should be possible to grow GaAs heterostructures on InP. Both compounds are structurally suitable for the creation of integrated devices and micro-machines. Currently, for small detectors of area 3.1 mm^2 and thickness 180 μm, FWHM spectral resolutions of ~ 2.5 and 9.2 keV have been achieved 5.9 and 59.54 keV, respectively, at a detector temperatures of $-60^\circ C$ [29]. At liquid nitrogen temperatures ($-170^\circ C$), these figures improve considerably to 911 eV at 5.9 keV and 2.5 keV at 59.54 keV [23].

For γ-ray applications, there has been some effort to develop the heavier compounds with limited success—particularly the lead, bismuth and thallium compounds from period 6 of the periodic table. For example, PbI_2 has been investigated as a stable alternative to HgI_2 since it does not exhibit a destructive phase change between the melting point and room temperature and its density is similar. Unfortunately, while present detectors yield good room temperature X-ray performance [30] (415 eV FWHM at 5.9 and 1.4 keV FWHM at 59.54 keV for a 1 mm^2 device), their transport properties are so poor that detectors thicker than ~ 200 μm cannot be produced and therefore there has been little incentive to develop PbI_2 for γ-ray applications over say HgI_2, or even lower Z compounds such as CdZnTe or GaAs. Additionally, PbI_2 is very soft with a layered crystal structure similar to HgI_2. Consequently, it is difficult to handle. Both bismuth tri-iodide (BiI_3) and bismuth tri-sulfide (Bi_2S_3) have been proposed [31,32] as γ-ray detection media in view of their high atomic number ($Z_{eff} \sim 60$) and high carrier mobilities (BiI_3—$\mu_e = 600\,cm^2\,V^{-1}\,s^{-1}$, $\mu_h = 20\,cm^2\,V^{-1}\,s^{-1}$; Bi_2S_3—$\mu_e = 1100\,cm^2\,V^{-1}\,s^{-1}$, $\mu_h = 200\,cm^2\,V^{-1}\,s^{-1}$). In fact, their photoelectric absorption cross-sections are about seven times that of CdTe or twice that of HgI_2 at 60 keV. Thin (100 μm) prototype BiI_3 detectors have shown a spectroscopic response to 5.8 MeV α-particles ($\Delta E = 2.2$ MeV), but no response to γ-rays [31]. Bi_2S_3 detectors, on the other hand, have shown a response to γ-radiation, although not spectroscopic [32]. For both compounds, problems with stoichiometry due to their complex crystal structure[5] has prevented further development.

Better results have been obtained with TlBr. Although this is a particularly soft material (Knoop hardness of 12 $kg\,mm^{-2}$—about the same hardness as refrigerated butter), FWHM room temperature energy resolutions of 1.8 keV at 5.9 keV and 3.3 keV at 59.5 keV have been obtained [33] for detectors of dimensions $2.8 \times 2.8 \times 0.8\,mm^3$. These resolutions were found to improve with decreasing temperature exhibiting a minimum near $-30^\circ C$. At this temperature, the FWHM energy resolutions were 800 eV at 5.9 keV and 2.3 keV at 59.54 keV, respectively. Although these detectors did not suffer from the stability problems normally associated with TlBr detectors [34], they did display polarization effects (i.e., time dependent changes in gain and spectral broadening), which were correlated with large energy depositions per unit time [33].

[5] Rhombohedral with each bismuth atom octahedrally coordinated with six iodine or sulfur atoms.

Numerous other compounds have been proposed (e.g., ZnSe [35], CdZnSe [36], CdMnTe [37], CdTeSe [38], $TlPbI_3$ [39], GaSe [40]). Of these, ZnSe, CdZnSe, CdTeSe and CdMnTe have produced spectroscopic results at X-ray wavelengths while GaSe and $TlPbI_3$ have shown a response to 5.48 MeV α-particles [40,41]. Although ZnSe, CdMnTe and CdTeSe are barely spectroscopic at this time, reasonable results have been obtained with CdZnSe (1.8 keV at 5.9 keV for a 3.1 mm^2, 2.5 mm thick device [36]).

5. Future development

γ-Ray spectroscopy should drive the future development of compound semiconductors, because material properties are critical for thick detectors and not so crucial for thin detectors. For example, for X-ray detection, lifetime–mobility products need only be 10^{-3} and 10^{-4} to ensure the efficient collection of carriers and near Fano limited energy resolution—provided detector thicknesses are kept below 200 μm. As such, X-ray applications are good for driving the development of the front-end electronics (and it should be borne in mind that detectors up to 200 μm thick still have nearly unity quantum efficiency up to 20 keV). For γ-ray applications, the objective should be to produce a detector, that will operate at, or above room temperature, with an FWHM energy resolution of 1% at 500 keV or less and a usable active volume of a cubic cm.

5.1. General requirements

In terms of general requirements, Z should be greater than 40 to yield a high stopping power. Structurally, the lattice should also have a close packed geometry (such as a body centered cubic structure) to optimize density. The material should have a low dielectric constant, to ensure low capacitance and therefore system noise. For practical systems preference should be given to binary or pseudo-alloyed binary systems over ternary or higher-order compounds, based on the multiplication of stoichiometry errors. Additionally, such a restriction would also "clean-up" the response function by reducing the number of "unwanted" absorption and emission features in the measured energy-loss spectra. The selection criteria can be further extended to exclude most II–VI compounds in view of their propensity for toxicity, deep trapping and polarization effects, coupled with their low melting points. The latter makes it difficult to perform the required thermal annealing to activate implanted dopants.

From an electronic point of view, the band-gap energy should be greater than 0.14 so there is no thermal generation of carriers at room temperature and the resistivity should be greater than $10^8\,\Omega$ cm to allow larger biases to be applied, resulting in faster drift velocities and deeper depletion depths. For the highest Z materials, Fano noise can also be substantially reduced (and hence energy resolution improved), by choosing compounds from groups n(period 6)-VIIB, where n = II, III or IV (e.g., HgI_2). This is illustrated in Fig. 6 in which we plot the band-gap energy as a function of electron–hole pair creation energy.[6] From the graph we see that the compounds HgI_2, PbI_2 and TlBr are clearly displaced from the line describing the bulk of the semiconductors, giving an $\sim$30% reduction in the mean pair creation energy for a given band gap compared to the main branch. Indeed, if the n(period 6)-VIIB relationship really exists, then BiI_3 should also lie on the second branch.

As pointed out by Armantrout et al. [22], a practical upper limit of $\sim$2.2 eV can be placed on the band-gap energy, based on the fact that carrier mobilities tend to drop rapidly with increasing band gap due to polar lattice scattering. In addition, heavy compounds in this category tend to be mechanically soft or layered making them difficult to handle. Consequently, they do not lend themselves to standard processing techniques, particularly array replication. Finally, electron and hole mobility–lifetime products should be better than 10^{-2} and 10^{-3}, respectively, to ensure good carrier transport and therefore spectral

[6] Strictly speaking, as pointed out by Klein [42], the term electron–hole pair creation energy is not only incorrect, but highly misleading. What is actually being considered is the average amount of energy consumed per pair.

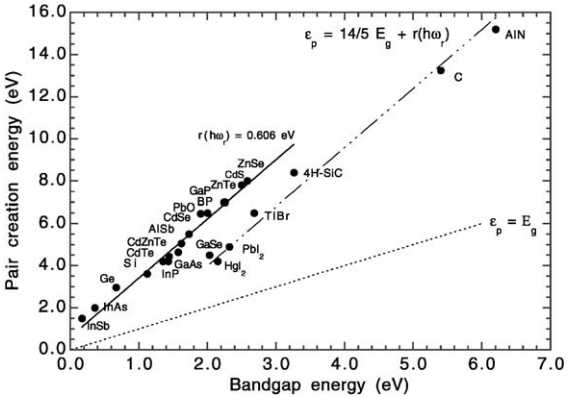

Fig. 6. Average energy to create an electron–hole pair as a function of band-gap energy for a selection of semiconductors. Two main bands are evident—the main branch found by Klein [42] (solid line) and the n-VIIB branch (dashed-dotted line). The dotted line denotes the limiting case when $\varepsilon_p = E_g$. The difference between this curve and the measured curves is due to optical phonon losses and the residual kinetic energy left over from impact ionization thresholding effects. Note the solid lines through the two branches are best fit "Klein functions" of the form $14/5\ E_g + a_1$ in which a_1 is a free parameter. In order to obtain good fits to both the main and secondary branches, both AlN and diamond were fit as part of the secondary branch because they are clearly displaced from the main branch. Note also, that while the parameter $a_1 = 0.6$ for the main branch is reasonable, in that it should lie in the range $0 \leqslant a_1 \leqslant 1.0$, the fitted value for the secondary branch is unphysical.

performance. This in turn, places a limit on the density of trapping centers of typically $< 5 \times 10^{12}\,\mathrm{cm}^{-3}$. Applying the above criteria reduces the number of acceptable compounds to about 10.

5.2. Recommended compounds

In terms of future material development, several materials are potentially very interesting. These are listed in Table 3 and were chosen to cover the widest range of applications, rather than a specific waveband.

AlSb was originally identified by Armantrout et al. [22] as the material with the greatest potential, in view of its high $Z(= 51)$, intermediate band gap (1.6 eV), ZB crystal structure, good electron mobility and very high hole mobility (which theoretically is at least five times larger than any other compound semiconductor). However, as it has proved difficult to grow due to the high affinity of Al to oxygen combined with the high volatility of Sb. Consequently, spectroscopic material has not been produced, although single crystal resistivities of up to $8 \times 10^5\,\Omega\,\mathrm{cm}$ have been reported [43].

Diamond has long been identified as a promising X-ray detection medium. However, its use has been limited by the inability to grow semiconductor grade material and by the difficulty in doping this extremely stable material. For thin detectors, ion implantation offers a promising approach to doping due to its ability to create non-equilibrium defects during the bombardment process. SiC has similar properties to diamond in that it is extremely hard, inert and chemically stable. In fact, SiC radiation detectors have been operated at temperatures of 200°C in high radiation fields without showing signs of degradation. It view of its similar properties and smaller band-gap energy (2.2 eV as opposed to 5.4 eV for diamond), SiC can be considered a high-resolution derivative of diamond. Recent work by Metzger et al. [44] using mixed radiation fields, supports their opinion that SiC diodes can be used for any type of radiation.

Of particular interest are group III-nitride compounds, InN, GaN and AlN. Nitrogen is a small atom and highly electronegative and as such makes an ideal constituent for III–V WBG semiconductors. Group III-N compounds offer a higher utilizable band-gap range, higher bonding strength, and better thermal conductivity. Aluminum nitride has the widest band-gap of any compound semiconductor and offers the potential of making "solar-blind" X-ray detectors, i.e., detectors insensitive to the solar visible and ultraviolet (UV) radiation. InN is predicted to have a low effective mass for electrons, which should lead to high mobilities and high saturation velocities. Early experimental work shows promise for exploiting these properties, since it is widely envisioned that InN might become the successor to GaN for high-power, high-temperature microwave and millimeter wave applications. At X-ray wavelengths very little work has been carried out. Although the first room temperature detectors have been produced, no results have been

Table 3
Suggested compounds for future development

Material	Band gap (eV)	Density ($g\,cm^{-3}$)	Comments	Space/medical/general applications
InSb	0.17	5.66	Narrow band-gap, three times better energy resolution than Si	High-resolution X-ray astronomy (He_3 temperatures), XRF
InAs	0.35	5.68	Narrow band-gap, two times better energy resolution than Si	High-resolution X-ray astronomy (He_3 temperatures), XRF
AlSb	1.62	4.26	Theoretically, the best all round performer	Room temperature Si replacement, compact planetary spectrometers
PbO	1.9	9.8	Highest Z, γ-ray detection	Compact γ-ray planetary detectors/radio-guided probes
cBP	2.0	2.90	Thermal neutron detection	Spacecraft in-orbit neutron monitor, neutron capture therapy
iB_4C	2.0	2.51	Thermal neutron detection—cross-section $\sim$4000 barns, 3rd hardest material	Spacecraft in-orbit neutron monitor, neutron capture therapy
III-N			High temperature ceramics, chemically inert, stable, range of band gaps	High temperature applications, planetary surfaces, solid-state lighting
InN	2.0 (0.7)[a]	6.81	High effective hole mass, high Z	Compact γ-ray spectrometer for planetary rovers
GaN	3.4	6.15	High mobility, high-speed applications	Solar X-ray monitors. Penetrators, synchrotron applications
cBN	6.1	3.48	Neutron detection, extremely radiation hard, second hardest material	Planetary surface neutron monitor, nuclear pile detectors
AlN	6.2	3.25	Widest band-gap, radiation hard	Solar blind X-ray monitors, well logging
CdMnTe	2.1	5.8	γ-Ray detection, inexpensive replacement for CdZnTe	γ-Ray astronomy, low-cost γ-ray imagers/PET detectors, well logging
4H-SiC	3.2	3.2	All round radiation detection (p, nγ) in extreme environments, rad hard	Planetary surface X-ray spectrometer, solar flare monitor, nuclear reactors
TlBr	2.68	7.56	High Z, γ-ray detection	γ-Ray astronomy/radio-guided probes, well logging
Diamond	5.4	3.52	High temperature, hardest material, chemically inert, radiation hard, robust, stable	Detectors for hot corrosive, atmospheres, solar flare monitors, hadron therapy—tissue equivalent detectors

Note: The prefixes c, i and 4H identify a particular crystal structure, i.e., cubic, icosahedral and four-plane hexagonal, respectively. Apart from AlSb and CdMnTe, which could become the workhorses of room temperature X- and γ-ray spectrometry, each material has great potential in a specific area. Even though diamond, SiC and TlBr are already under investigation, we include them here for future development because of their immaturity.

[a] See text.

reported. However, any lack of success may not be entirely unexpected since most recently Davydov et al. [45] have reported finding a well pronounced photoluminescence band close to the absorption edge. In essence, the band-gap energy of InN may be 0.7 eV and not the generally accepted value of 2.0 eV. In the short term, GaN might be the easiest nitride to investigate since its Fermi-level is not completely pinned and as such, for n-type material, it should be possible to find a range of contact materials for which $\phi_m < \phi_s$. Recently, Vaitkus et al. [46] have demonstrated that a thin (2.5 μm thick), 1.77 mm^2 epitaxial GaN pad detector has shown a response to α-particles.

Boron nitride (BN), boron phosphide (BP) and boron carbide (B_4C) are three compounds that would make ideal room temperature thermal neutron detectors that could replace bulky and inefficient ^3He and BF_3 gas-based systems. The principal reaction mechanism in both compounds is $^{10}B(n, \alpha)^7Li$ which has a cross-section of 3840 barns. Since the Q value for the dominant decay to the first excited state is 2.31 MeV, over 10^5 electron–hole pairs would be generated for each captured neutron. Thus, given that the range of the reaction products is negligible, a solid-state device which acts as both absorber and detector would be highly compact and efficient. Additionally, since their densities are relatively low, the background from γ-rays (which invariably accompany neutron production) will also be low. BP, B_4C and BN are refractory materials and chemically inert and at this time are being actively developed for high-temperature/high-power electronic applications. The phosphide has a cubic ZB structure, while the nitride and carbide are available in three phases—cubic, hexagonal and amorphous. Until recently, impurities have prevented the production of detector quality monocrystalline material [47]. However, Ananthanarayanan et al. [48] have demonstrated that small 6.4 mm diameter, 1 mm thick polycrystalline BP and BN detectors are responsive to thermal neutron fluxes of $10^8\,cm^{-2}\,s^{-1}$. Most recently, there has been a breakthrough in the production mono-crystalline material for all three boron compounds. Zhang et al. [49] have reported the production of cubic BN films, Kumashiro [50] has reported the production of single crystalline BP wafers and Robertson et al. [51] have reported direct neutron detection with B_5C.

TlBr is recommended because of its great potential as a γ-ray detector. Although some work has been carried out and promising results obtained [32], we include it here because its transport properties are still plagued by material problems. Currently, detector thickness are limited to ~1 mm by poor hole transport. Other potential γ-ray materials are difficult to identify, because, as the effective Z increases (which is essential for efficient γ-ray detection), two detrimental effects emerge—particularly as we move from III–V compounds into II–VI compounds. The first is that the material becomes softer and generally layered and therefore difficult to work with and the second, the mobilities (and particularly hole mobilities) decrease markedly. However, in spite of this, potential candidates emerge—although probably because one or more of these critical parameters are unknown. For example, CdMnTe is particularly interesting as a potential replacement to CdZnTe. It is easier to engineer the band-gap energy. This is illustrated in Fig. 4 from which we can see that for the possible ranges of alloying, the lattice strain is considerable less than for CdZnTe and that a much larger variation in band-gap energies is available. In fact, the addition of Mn linearly increases the room temperature band-gap at a rate of 13 meV per %, which has more than twice the effect of Zn alloying. An added benefit is that, unlike Zn, the segregation of Mn along the growth axis is almost non-existent and the lattice is strengthened. Lastly, CdMnTe can be produced by the modified Bridgeman technique, which is considerably less complicated and expensive than the High Pressure Bridgeman method used to produce CdZnTe. To date, most research has centered on Faraday rotation and magnetic sensor applications, since CdMnTe is also a dilute magnetic semiconductor. However, the first X-ray detection systems have been fabricated, although the X-ray performance is poor with FWHM resolutions of 21 keV at 59.54 keV being reported for a device of area 1.8 mm^2 and thickness 500 μm [35]. PbO is also interesting in view on its extreme density ($9.8\,g\,cm^{-3}$) and favorable band-gap

energy (2.2 eV). However, it is unclear if it would make a good γ-ray detection medium, since there is virtually no information on its transport properties.

Lastly, we have also included two NBG materials, InAs and InSb, in our list, since both offer the possibility of spectral resolutions beyond the elemental semiconductors, toward the superconductors. Potentially, InAs can offer twice the energy resolution of silicon and InSb three times. In addition both have very high electron mobilities, which offer the potential of low bias operation. The main disadvantage of these compounds is that they will require cryogenic cooling. However, both are extensively used in the semiconductor industry and while X-ray sensitive detectors have yet to be produced, there has been the first report of the detection of high-energy α-particles by a small InSb device operated at a temperature of 4.2 K [15].

6. Discussion and conclusions

While the performances of most compound semiconductors are not yet close to the Fano limit, in practice they are close enough to satisfy the requirements of many anticipated applications in nuclear medicine, environmental redemption and space science. In Table 4, we list some of the best resolutions reported. For completeness, we also list the resolutions at room temperature where possible, since there are many applications in which resolving power is not a primary requirement, e.g., dosimetry. Note, the figures are quoted for the collection of both carriers. Spectral enhancement techniques involving single carrier collection have not been employed. We also list resolutions obtained for pixel detectors, i.e., detectors whose area and thickness have been optimized[7] to maximize carrier transport and match input FET and detector capacitance. While these detectors are usually too small to be useful for most applications, the figures are useful in that they indicate the performance that can be potentially achieved. However, it should be noted, that while HgI_2, PbI_2 and TlBr are primarily being developed for hard X- and γ-ray applications, they also make surprisingly good soft X-ray detectors with usable sub-keV responses down to ~1 keV, e.g., Refs. [30,33,58]. Indeed, a 5 mm^2, 200 μm thick HgI_2 detector, operated at room temperature, has displayed near Fano performance at 5.9 keV [57] ($\Delta E = 198$ eV FWHM).

Hole collection problems currently limit the useful thickness (and ultimately high energy performance) of compound semiconductor detectors to about 0.2–1.0 mm. For low-noise systems, the thickness of the detector must also be traded-off with detector capacitance, which directly affects the electronic noise of the system. For practical detection systems, the best performance figures are achieved with substantial cooling to reduce the detector electronic noise or enhance carrier mobilities. Though with worse resolution, compound semiconductors can operate at higher temperatures. For example, SiC is still spectroscopic up to +100°C [25] ($\Delta E = 1.1$ keV at 59.54 keV), CdTe up to a temperature of +92°C [59] ($\Delta E = 53$ keV at 122 keV), CdZnTe up to a temperature of +70°C [60] ($\Delta E = 9.4$ keV at 32 keV), HgI_2 detectors have been operated to +65°C [61] ($\Delta E = 1400$ eV at 59.54 keV) and PbI_2 to +100°C [62] ($\Delta E = 1.2$ keV at 5.9 keV). However, the fact that the performance of most compounds can be significantly improved with only modest cooling has important consequences for medical and space applications where power, mass and volume are at a premium. Such cooling can be readily achieved with Peltier systems or for space applications, small passive radiator panels alleviating the need for complex and expensive cryogenic systems—as in the case of Ge detectors. Lastly, we note that for the compounds with the poorest hole transport, stability and time dependent effects in the detectors response are still problematic. For HgI_2, this manifests itself in a gradual improvement in energy resolution after bias is applied [63], whereas, for TlBr the spectra degrade in gain and energy resolution when the total energy deposition per unit time exceeds a threshold [33]. II–VI materials are particularly prone to polarization effects, which are believed to arise from deep, long-lived traps that perturb and

[7] But not to the extent of promoting the small-pixel effect, as described in Barrett et al. [18].

Table 4
Best energy resolutions achieved with prototype compound semiconductor detectors

Material	Detector size Area × thickness	FWHM ΔE at 5.9 keV (eV)	FWHM ΔE at 59.5 keV (eV)	Reference
Si	0.8 mm^2, 500 μm	245 at −15°C	524 at −15°C	[23]
		750 at +15°C	800 at +15°C	[23]
Si(Li) drift	16 mm^2, 3.5 mm	175 at −90°C	430 at −90°C	[52]
4H SiC	2 mm^2, 30 μm	—	2700 at RT	[23]
4H SiC (pixel)	0.3 mm^2, 50 μm	—	693 at RT	[25]
			1100 at +100°C	
Ge	30 mm^2, 5 mm	150 at −170°C	—	[53]
GaAs	0.8 mm^2, 40 μm	450 at −22°C	670 at −22°C	[23]
		572 at RT	780 at RT	
GaAs (pixel)	250 × 250 × 40 μm^3	219 at −30°C	468 at −30°C	[54]
		266 at RT	487 at RT	
InP	3.142 mm^2, 200 μm	911 at −170°C	3050 at −170°C	[29]
		2480 at −60°C	920 at −60°C	[23]
CdTe	16 mm^2, 1.2 mm	310 at −60°C	600 at −60°C	[52]
$Cd_{(1-x)}Mn_xTe$ x=0.55	1.8 mm^2, 500 μm	—	21230 at RT	[36]
$Cd_{(1-x)}Zn_xTe$ x=0.1	3.142 mm^2, 2.5 mm	311 at −37°C	824 at −37°C	[55]
		1508 at RT	2900 at RT	
CdSe	2 mm^2, 0.12 mm	1400 at RT	8500 at RT	[56]
$Cd_{(1-x)}Zn_xSe$ x=0.3	3.142 mm^2, 2.5 mm	1800 at RT	—	[38]
$CdTe_{(1-x)}Se_x$ x=0.1	100 mm^2, 1 mm	—	6000 at RT	[37]
HgI_2 det 1	5 mm^2, 200 μm	198 at 0°C	650 at 0°C	[57]
det 2	7 mm^2, 500 μm	600 at RT	2400 at RT	[58]
PbI_2	1 mm^2, 50 μm	415 at RT	1380 at RT	[30]
TlBr	3.142 mm^2, 800 μm	800 at −30°C	2300 at −30°C	[33]
		1800 at RT	3300 at RT	

Note: The measurements were carried out under uniform illumination using ^{55}Fe and ^{241}Am radioactive sources. The figures are quoted for the collection of both carriers. Spectral enhancement techniques involving single carrier collection have not been employed. The equivalent FWHM pulser resolutions (where given) were 220 eV (Si), 2700 eV (SiC), 415 eV (SiC pixel), 400 eV (GaAs1), (GaAs pixel), 163 eV, 760 eV (InP), 290 eV (CdTe), (CdZnTe), 1100 eV (CdSe), 1100 (CdZnSe), 152 eV (HgI_2 det 1), 343 eV (HgI_2 det 2) and 574 eV (TlBr). For completeness, we also list the resolutions at room temperature (RT) were possible, since there are many applications in which resolving power is not a primary requirement.

distort the local electric field leading to time dependent charge collection problems.

6.1. The longer term

In the preceding sections we have concentrated purely on material developments. In the longer term, material improvements must be paralleled by corresponding developments in heterostructure and quantum heterostructure technology, provided of course, strain is not a limiting factor. Doping a semiconductor like Si or GaAs provides control over the sign and density of the charge carriers. By combining different semiconductors in heterostructures, one gains control over much more, including the band-gap energy, refractive index, carrier mass and mobility, and other fundamental parameters. For example, heterostructures may solve the problem of contacting by building up a series of semiconductor layers until it is possible to satisfy the relationship that the work function of the metal contact is less than that of the semiconductor (i.e., $\phi_m < \phi_s$) for n-type material. An alternate approach is to use a so-called "interface control layer" at the junction been the contact and the semiconductor. It has

been shown that such a layer can lower the overall SBH allowing better contacting to wide band-gap semiconductors [64]. The reduction in barrier height is accomplished largely through the breakdown of one large (Schottky) barrier height into two smaller ones (an SBH and a heterojunction band-offset).

In principal, quantum heterostructures could also facilitate ultra-low-noise operation by constructing a series of quantum valleys, which have the dimensions of the order of 0.1 nm at the contact side and millimeters or even centimeters on the intrinsic-layer side. As such, the readout would have approximately the dimensions of the readout node of a Si CCD, which is directly responsible for their ultra-low-noise operation. The basis of operation is based on the work of Esaki and Tsu [65], who suggested that it would be possible to grow alternating layers of GaAs and AlGaAs in a periodic array to form a super-lattice, which would have remarkably different electronic properties from those of bulk GaAs or AlGaAs. When a layer of GaAs is sandwiched between two "infinite" layers of AlGaAs, the carriers in the GaAs are trapped in the GaAs layer along the growth direction. In this structure, the energy levels in the well are raised in the conduction band for the electrons and lowered in the valence band for the holes. This leads to the confinement of electrons along the growth direction and characterizes the well as a structure that has a 1-D confinement for charged carriers. The composite of many such layers would form a bi-periodic array of rectangular quantum wires. At the present time, the first purpose-built heterostructures for X-ray applications are being reported in the literature. For example, Silenas et al. [66] have constructed an n-GaAs–p-AlGaAs graded-gap X-ray detector in which the AlGaAs layer functions as the classical absorption and detection layer and the n-GaAs layer as a carrier multiplication zone. Early results show the device is sensitive to α-particles and gains of up to 100 can be achieved.

Perhaps even more speculative, we note reports of porosity in III–V compounds, particularly, GaAs, GaP and InP [67]. While one can envision photonic crystal applications, depending on cytotoxicity, this also leads to the possibility of animal cell: semiconductor interfacing as in the case of nanostructured Si [68].

Acknowledgements

The IHP-contract HPRI-CT-1999-00040 of the European Commission supported part of this work.

References

[1] P.J. Van Heerden, The crystal counter, Dissertation, Utrecht University, 1945.
[2] R. Hofstadter, Nucleonics 4 (2) (1949) 27.
[3] K. McKay, Phys. Rev. 76 (1949) 1537.
[4] M.B. Prince, P. Polishuk, IEEE Trans. Nucl. Sci. NS-14 (1967) 537.
[5] D.S. McGregor, H. Harmon, Nucl. Instr. and Meth. A 395 (1997) 101.
[6] W. Shockley, J. Appl. Phys. 9 (1938) 635.
[7] S. Ramo, Proc. IRE 27 (1939) 584.
[8] K. Hecht, Z. Phys. 77 (1932) 235.
[9] R. Trammell, F.J. Walter, Nucl. Instr. and Meth. 76 (1969) 317.
[10] W. Faschinger, in: S. Pearton (Ed.), Wide Bandgap Semiconductors, William Andrew Publishing, New York, 1999, pp. 1–37.
[11] D. Olega, J. Faurie, S. Sivananthan, P. Raccah, App. Phys. Lett. 47 (1985) 1172.
[12] J.E. Toney, T.E. Schlesinger, R.B. James, Nucl. Inst. and Meth. A 428 (1999) 14.
[13] A.W. Webb, S.B. Quadri, E.R. Carpenter, E.F. Skelton, J. Appl. Phys. 61 (1987) 2492.
[14] J.F. Butler, C.L. Lingren, F.P. Doty, IEEE Trans. Nucl. Sci. NS39 (1992) 605.
[15] I. Kanno, F. Yoshihara, R. Nouchi, O. Sugiura, T. Nakamura, M. Katagiri, Rev. Sci. Instr. 73 (2002) 1.
[16] M.R. Squillante, G. Entine, Nucl. Instr. and Meth. A 380 (1996) 160.
[17] P.N. Luke, IEEE Trans. Nucl. Sci. NS-32 (1985) 556.
[18] H. Barrett, J. Eskin, H. Barber, Phys. Rev. Lett. 75 (1995) 156.
[19] L.J. Brillson, Contacts to Semiconductors: Fundamentals and Technology, Noyes Publishing Co., Park Ridge, NJ, 1993.
[20] T.-J. Kim, P.H. Holloway, in: S. Pearton (Ed.), Wide Bandgap Semiconductors, William Andrew Publishing, New York, 1999, pp. 80–150.
[21] A.G. Baca, F. Ren, J.C. Zolper, R.D. Briggs, S.J. Pearton, Thin Solid Films 308 (1997) 599.

[22] G. Armantrout, S. Swierkowski, J. Sherohman, J. Yee, IEEE Trans. Nucl. Sci. NS-24 (1977) 121.
[23] A. Owens, A. Peacock, M. Bavdaz, Proc. SPIE 4851 (2003) 1059.
[24] G. Bertuccio, R. Casiraghi, F. Nava, IEEE Trans. Nucl. Sci. NS-481 (2001) 232.
[25] G. Bertuccio, R. Casiraghi, E. Gatti, D. Maiocchi, F. Nava, C. Canali, A. Cetronio, C. Lanzieri, Mater. Sci. Forum 433–436 (2003) 941.
[26] P. Bergonzo, A. Brambilla, D. Tromson, C. Mer, B. Guizard, R. Marshall, F. Foulon, Nucl. Instr. and Meth. A 476 (2002) 694.
[27] A. Mainwood, Diam. Relat. Mater. 7 (1998) 504.
[28] F. Nava, C. Canali, M. Artuso, E. Gatti, P.F. Manfredi, S.F. Kozlov, IEEE Trans. Nucl. Sci. NS-26 (1979) 308.
[29] A. Owens, M. Bavdaz, V. Gostilo, D. Gryaznov, A. Loupilov, A. Peacock, H. Sipila, Nucl. Instr. and Meth. A 487 (2002) 167.
[30] K. Shah, F. Olschner, L. Moy, P. Bennett, M. Misra, J. Zhang, M. Squillante, J. Lund, Nucl. Instr. and Meth. A 380 (1996) 266.
[31] M. Matsumoto, K. Hitomi, T. Shoji, Y. Hiratate, IEEE Trans. Nucl. Sci. NS-49 (2002) 2517.
[32] F.V. Wald, J. Bullitt, R.O. Bell, IEEE Trans. Nucl. Sci. NS-22 (1975) 246.
[33] A. Owens, M. Bavdaz, G. Brammertz, G. Gostilo, H. Graafsma, M. Krumrey, I. Lisjutin, A. Peacock, A. Puig, H. Sipila, S. Zatoloka, Nucl. Instr. and Meth. A 497 (2003) 370.
[34] A. Owens, M. Bavdaz, I. Lisjutun, A. Peacock, S. Zatoloka, Nucl. Instr. and Meth. A 458 (2001) 413.
[35] E.E. Eissler, K.G. Lynn, IEEE Trans. Nucl. Sci. NS42 (1995) 663.
[36] A. Burger, M. Roth, M. Schieber, IEEE Trans. Nucl. Sci. NS-32 (1985) 556.
[37] A. Burger, K. Chattopadhyay, H. Chen, J.O. Ndap, X. Ma, S. Trivedi, S.W. Kutcher, R. Chen, R.D. Rosemeier, J. Cryst. Growth 198/199 (1999) 872.
[38] M. Fiederle, D. Ebling, C. Eiche, D.M. Hofmann, M. Salk, W. Stadler, K. Benz, B.K. Meyer, J. Cryst. Growth 138 (1994) 529.
[39] M. Kocsis, IEEE Trans. Nucl. Sci. NS47 (2000) 1945.
[40] C. Manfredotti, R. Murri, L. Vasanelli, Nucl. Instr. and Meth. A 115 (1974) 349.
[41] K. Hitomi, T. Onodero, T. Shoji, Y. Hiratate, IEEE Trans. Nucl. Sci. NS50 (2003) 1039.
[42] C.A. Klein, J. Appl. Phys. 4 (1968) 2029.
[43] V.E. Kutny, A.V. Rybka, A.S. Abyzov, L.N. Davydov, V.K. Komar, M.S. Rowland, C.F. Smith, Nucl. Instr. and Meth. A 458 (2001) 448.
[44] S. Metzger, H. Henschel, O. Köhn, W. Lennartz, IEEE Trans. Nucl. Sci. NS-49 (2002) 1351.
[45] V.Yu. Davydov, A.A. Klochikhin, R.P. Seisyan, V.V. Emtsev, S.V. Ivanov, F. Bechstedt, J. Furthmüller, H. Harima, A.V. Mudryi, J. Aderhold, O. Semchinova, J. Graul, J. Phys. Status Solidi (B) 229 (2002) R1.
[46] J. Vaitkus, W. Cunningham, E. Gaubas, M. Rahman, S. Sakai, K. Smith, T. Wang, Nucl. Instr. and Meth. A 509 (2003) 60.
[47] T. Viles, B. Brunett, H. Yoon, J.C. Lund, H. Hermon, D. Buchenauer, K. McCarty, M. Cliff, D. Dible, R.B. James, Mater. Res. Soc. Symp. Proc. 487 (1998) 585.
[48] K.P. Ananthanarayanan, P.J. Gilisse, A. Choudry, Nucl. Instr. and Meth. A 118 (1974) 45.
[49] X.W. Zhang, H.-G. Boyen, N. Deyneka, P. Ziemann, F. Banhart, M. Schreck, Nat. Mater. 2 (2003) 312.
[50] Y. Kumashiro, J. Mater. Res. 5 (1996) 2933.
[51] B.W. Robertson, S. Adenwalla, A. Harken, P. Welsch, J.I. Brand, P.A. Dowben, J.P. Claassen, Appl. Phys. Lett. 80 (2002) 3644.
[52] A. Loupilov, A. Sokolov, V. Gostilo, J. Radiat. Phys. Chem. 61 (2001) 463.
[53] http://www.bsi.lv/products/13.htm.
[54] A. Owens, M. Bavdaz, A. Peacock, A. Poelaert, H. Andersson, S. Nenonen, L. Tröger, G. Bertuccio, J. App. Phys. 90 (2001) 5376.
[55] A. Owens, M. Bavdaz, H. Andersson, T. Gagliardi, M. Krumrey, S. Nenonen, A. Peacock, I. Taylor, Nucl. Instr. and Meth. A 484 (2002) 242.
[56] M. Roth, Nucl. Instr. and Meth. A 283 (1989) 291.
[57] S. Iwanczyk, Y.J. Yang, J.G. Bradley, J.M. Conley, A.L. Albee, T.E. Economou, IEEE Trans. Nucl. Sci. NS-36 (1989) 841.
[58] A. Owens, M. Bavdaz, G. Brammertz, M. Krumrey, D. Martin, A. Peacock, L. Tröger, Nucl. Instr. and Meth. A 479 (2002) 535.
[59] M.R. Squillante, G. Entine, Nucl. Instr. and Meth. A 380 (1996) 160.
[60] S.U. Egarievwe, K.T. Chen, A. Burger, R.B. James, C.M. Lisse, J. X-ray Sci. Technol. 6 (1996) 309.
[61] F.P. Vaccaro, L. van den Berg, R.D. Vigil, R.P. DeVito, C.R. Johnson, Submitted to the 12th International Workshop on Room-temperature X- and Gamma-Ray Detectors, IEEE NSS/MIS Conference, November 2001.
[62] J.C. Lund, K. Shah, F. Olschner, J. Zhang, L. Moy, S. Medrick, M. Squillante, Nucl. Instr. and Meth. A 322 (1992) 464.
[63] V. Gerrish, Nucl. Instr. and Meth. A 322 (1992) 402.
[64] A. Vilan, A. Ahanzer, D. Cahen, Nature 404 (2000) 166.
[65] L. Esaki, R. Tsu, IBM J. Res. Dev. 24 (1970) 61.
[66] S. Silenas, K. Pozela, L. Dapkus, V. Jasutis, V. Juciene, J. Pozela, K. Smith, Nucl. Instr. and Meth. A 509 (2003) 30.
[67] H. Föll, J. Carstensen, S. Langa, M. Christopherson, I.M. Tiginyanu, Phys. Status Solidi (A) 197 (2003) 61.
[68] S.C. Bayliss, P.J. Harris, L.D. Buckberry, C. Rousseau, J. Mater. Sci. Lett. 17 (1997) 737.